Excitons in type-II quantum dots: Finite offsets

U. E. H. Laheld,* F. B. Pedersen,† and P. C. Hemmer‡
Institutt for Fysikk, Norges Tekniske Høgskole, N-7034 Trondheim, Norway
(Received 1 November 1994)

Quantum size effects for an exciton attached to a spherical quantum dot are calculated by a variational approach. The band lineups are assumed to be type II with finite offsets V_e and V_h. The dependence of the exciton binding energy upon the dot radius R and the offsets is studied for different sets of electron and hole effective masses.

I. INTRODUCTION

With the development of experimental techniques for fabrication of semiconductor heterostructures, quantum-size effects in these low-dimensional structures (quantum wells,[1–7] wires[8] and dots[9,10]) have been studied extensively.[11] The quantum state of an Wannier exciton is one main subject in this respect, since, by the spatial confinement in these microstructures, it is qualitatively different from the exciton state in bulk materials.

Several theoretical studies, with various degrees of sophistication, exist for excitons in type-I heterostructures for quantum wells, quantum wires, and quantum dots. Excitons in type-II heterostructures have also been studied,[9,10,12,13] but to a much lesser extent. A fundamental feature of type-II heterojunctions is the spatial separation of electron and hole, which leads to longer radiative lifetimes, lower exciton binding energy, and unusual dynamic and recombination properties of charge carriers as compared with type I. For an overview, including potential applications, we refer to a recent article,[14] from which we quote: "Though some III-V, IV-VI, and II-VI semiconductor materials can form type II junctions (AlInAs/InP, InAsSb/InSb, InAs/GaSb, GaInAsSb/GaSb, InGaAs/GaAsSb, Si/Ge, ZnTe/ZnSe, etc.) the intriguing properties of these remarkable structures are still poorly understood."

The case of excitons in type-II quantum dots has only recently been considered in two model calculations. Rorison[15] has used a simple separable wave function in a variational calculation, with parameters appropriate for GaAs/AlAs and InAs/GaSb dots. We[16] have, on the other hand, used a more sophisticated variational wave function, and also presented analytical considerations of limiting cases, with the aim of obtaining insight into how the exciton binding energy and the electron-hole correlations depend upon the effective masses and the dot radius. In Ref. 16, the offsets were assumed to be infinite, corresponding to a complete spatial separation of the electron and hole. It was shown that two different regimes exist: For dot radii R much smaller than the effective bulk Bohr radius the electron and hole are essentially uncorrelated, while for R much larger than the Bohr radius the electron and hole are strongly spatially correlated, residing near the dot boundary just opposite each other.

This infinite barrier model is artificial for small dot radii R, since in realistic situations the confined particle then tends to leak out in the barrier material. Moreover, the importance of the incomplete confinement in optical experiments is very clear, since the oscillator strength for excitonic transitions is proportional to the square of the electron-hole wave-function overlap. Thus, it will be worthwhile to make clear the dependence of the exciton binding energy, and of the wave function overlap, on the magnitudes of the offsets. For estimates of band offsets and effective masses for several III-V heterostructures see Refs. 14, 17, and 18.

In this work, we report the result of a variational calculation of the binding energy for the electron-hole system with *finite* offsets. Since it is always useful to have results for limiting cases to compare with, we compute first binding energies for the case in which one particle is confined, and the other completely free, i.e., $V_h = 0$. Since zero offset for one of the particles is a situation intermediate between a type-I and a type-II heterostructure, we denote this special case as being of type I$\frac{1}{2}$. A limiting type-I$\frac{1}{2}$ situation occurs when the confined particle is *completely* confined within the dot ($V_e = \infty$). In Sec. III, the dependence of the exciton binding energy upon the dot radius, the offsets, and the effective-mass values is studied, while Sec. IV contains results for the electron-hole overlap in the wave function, an important factor for the magnitude of oscillator strengths. We summarize our findings in Sec. V.

II. MODEL AND METHOD

In the effective-mass treatment the Hamiltonian for the electron-hole pair, which forms the exciton, is given by

$$H = \frac{p_e^2}{2m_e} + \frac{p_h^2}{2m_h} - \frac{e^2}{4\pi\epsilon}\frac{1}{|\mathbf{r}_e - \mathbf{r}_h|} + V_e(\mathbf{r}_e) + V_h(\mathbf{r}_h), \tag{1}$$

where

$$V_e(\mathbf{r}) = \begin{cases} 0 & \text{for } r \le R \\ V_e & \text{for } r > R \end{cases} \tag{2}$$

and

$$V_h(\mathbf{r}) = \begin{cases} V_h & \text{for } r \le R \\ 0 & \text{for } r > R. \end{cases} \quad (3)$$

Type-II situations correspond to V_e and V_h having the same sign. For definiteness, we assume both positive so that the electron is the confined particle. The alternative configuration presents, of course the same computational problem.

For simplicity, we have assumed the same electron (and hole) effective mass in the dot and the barrier material, and that the dielectric constants of the two media can be accounted for by a single average value ϵ. With degenerate valence band, we let m_h be either the heavy-hole or the light-hole effective mass, thus neglecting the complications due to the off-diagonal terms in the Kohn-Luttinger Hamiltonian.[19]

The main task is now to determine the ground-state energy E_0 of the Hamiltonian (1). The binding energy E_b of the exciton is then the energy required to remove the hole, given by the difference between E_0 and the confinement energy E_c, the ground-state energy of the electron in the spherical dot:

$$E_b = E_c - E_0. \quad (4)$$

As units of energy and length, we use an effective Rydberg energy,

$$E^h_{\mathrm{Ry}} = \frac{m_h}{2\hbar^2}\left(\frac{e^2}{4\pi\epsilon}\right)^2, \quad (5)$$

and an effective Bohr radius,

$$a_h = \frac{4\pi\epsilon\hbar^2}{m_h e^2}, \quad (6)$$

both in terms of the hole mass. In terms of these quantities, we denote

$$\hat{E} = \frac{E}{E^h_{\mathrm{Ry}}} \quad (7)$$

as our dimensionless energy, and

$$\hat{R} = \frac{R}{a_h} \quad (8)$$

as the dimensionless radius.

The ground-state energy of the Hamiltonian (1) is determined variationally, using the following nonorthogonal basis set of functions:

$$\psi(\mathbf{r}_e, \mathbf{r}_h) = \sum_{k=1}^{N_e}\sum_{l=1}^{N_h} C_{kl}\, e^{-k\eta r_e^2}\, e^{-l\gamma r_h}\, e^{-\beta|\mathbf{r}_e - \mathbf{r}_h|}. \quad (9)$$

The variational parameters are η, γ, β, and the expansion coefficients C_{kl}, altogether $3 + N_eN_h$ parameters. Optimalization, with respect to the expansion coefficients C_{kl}, is a generalized eigenvalue problem, consisting in diagonalization of a matrix of size $N_eN_h \times N_eN_h$. All matrix elements can be evaluated analytically in terms of error functions. The only numerical problems that need special attention arise because the analytic expressions contain terms that individually diverge when $\gamma_k + \gamma_l - 2\beta$ is close to zero, or because exponential terms may become inadmissably large for small ηs. Finally, the minimalization with respect to η, γ, and β is demanding, due to the existence of many local minima.

TABLE I. Exciton energy $\hat{E}_0$ for different basis set sizes. Here, $\hat{R} = 2$, $m_e = m_h$, and $\hat{V}_e = \hat{V}_h = 5$.

$N_e \backslash N_h$	1	2	3	4	5
1	1.505	1.406	1.381	1.377	1.376
2	1.467	1.368	1.343	1.339	1.338
3	1.460	1.361	1.336	1.332	1.331
4	1.457	1.359	1.333	1.329	
5	1.456	1.357	1.331		

Good accuracy is usually achieved with a moderate size of the basis set. This is illustrated by Table I, which shows, by means of a special example, how the result for the ground-state energy of the exciton depends upon the size of the basis set. Apparently a basis set of nine functions ($N_e = N_h = 3$) suffices to give the energy within 1% accuracy. The exceptional cases occur for very large offsets, because one cannot achieve an almost vanishing wave function in the nearly inaccessible region with a small number of basis functions, and for large dot radius R when the exciton is located near the boundary. In these special cases, we make use of alternative functional forms, as discussed below.

One may of course also check the quality of the Gaussian basis set for the confined particle by comparing the one-electron energies computed variationally with the known exact ground state. With $N_e = 5$, the accuracy is, in general, on the 1% level, or better. Although the confinement energy E_c in Eq. (4) may be obtained exactly, we compute it variationally for better procedural consistency.

III. EXCITON BINDING ENERGY

We first discuss the case of one particle confined to the dot material, with the other free to move. We denote this situation, intermediate between a type-I and a type-II heterostructure, as type $\mathrm{I}\frac{1}{2}$. Two examples of heterostructures with very small valence-band offsets are InAs/AlSb (Ref. 20) and $\mathrm{ZnSe/Zn_{0.79}Mn_{0.21}Se}$ (Ref. 21).

A negligible hole offset, and a *completely* confined electron constitutes the extreme case.

A. $V_e = \infty$, $V_h = 0$

For this extreme case we use, for the reason mentioned above, an alternative variational function,

$$\psi(\mathbf{r}_e, \mathbf{r}_h) = \frac{\sin(\pi r_e/R)}{r_e}\, e^{-\gamma r_h}\, e^{-\beta|\mathbf{r}_e - \mathbf{r}_h|}, \quad (10)$$

for $r_e \le R$, zero otherwise. The numerical results for the exciton binding energy E_b are shown in Fig. 1. Figure 2

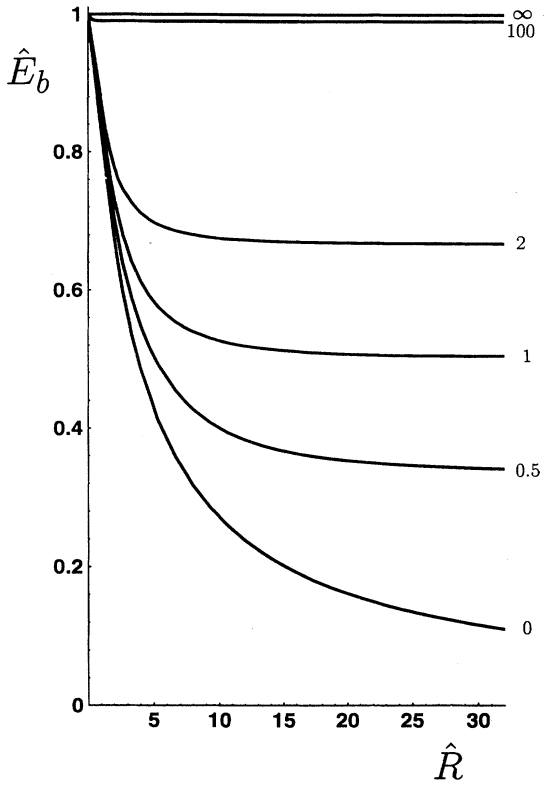

FIG. 1. The dimensionless exciton binding energy $\hat{E}_b$ for the offsets $V_e = \infty$, $V_h = 0$, as a function of the dimensionless dot radius $\hat{R} = R/a_h$. The values of the mass ratio m_e/m_h are shown on the right-hand side.

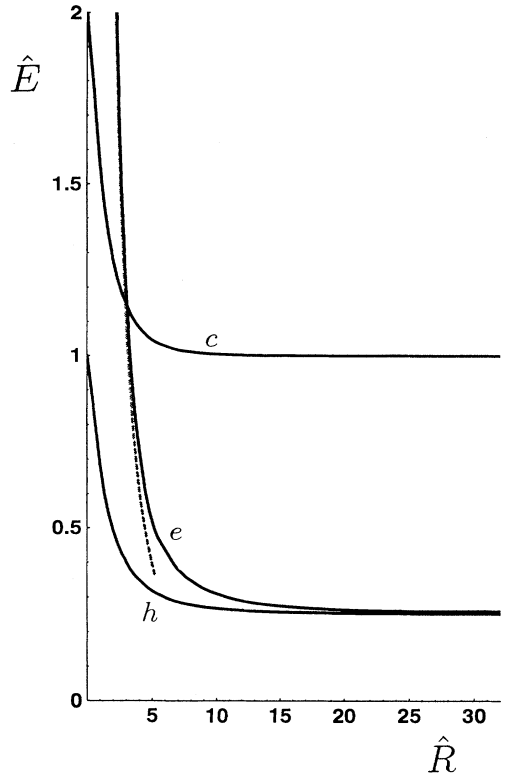

FIG. 2. The electron kinetic energy (e), the hole kinetic energy (h), and the absolute value of the Coulomb energy (c), as functions of the dimensionless quantum dot radius $\hat{R}$. These three contributions to the total energy are measured in the effective Rydberg (5). Here, $m_e = m_h$, $V_e = \infty$, and $V_h = 0$. The dashed line corresponds to the ground state of the single electron.

exhibits the size effect of the three different contributions to the total energy, viz., the kinetic energies of the electron and hole and the Coulomb interaction energy. We see that for $\hat{R}$ smaller than about 3 the electron kinetic energy is essentially equal to the ground-state energy in the dot, and dominates the other energy contributions. For large $\hat{R}$, the three energy contributions approach the ratio 1:1:-4, characteristic of the two-particle problem in bulk.

It is possible to understand the large-R and small-R behavior of the binding energy in Fig. 1. For large radii, the binding energy must approach the bulk binding energy with a *reduced* mass:

$$\hat{E}_b(R \to \infty) = \frac{m_e}{m_e + m_h}. \tag{11}$$

For small enough dot radius, or small electron to hole mass ratio ($\hat{R}^2 m_e/m_h \ll 1$), the electron will reside in its ground state $\psi_0(r_e) = \sin(\pi r_e/R)/(r_e\sqrt{2\pi R})$. Then the hole will see a charge distribution $\rho(r) = -e\psi_0^2(r)$, corresponding to a potential

$$V(r) = \int \frac{e\rho(r_e)}{4\pi\epsilon|\mathbf{r} - \mathbf{r}_e|} d^3 r_e = \begin{cases} -\dfrac{e^2}{4\pi\epsilon\, r} & \text{for } r > R \\ -\dfrac{e^2}{4\pi\epsilon R}\left[1 - \dfrac{R}{2\pi r}\sin\dfrac{2\pi r}{R} + 2\displaystyle\int_{r/R}^{1} \sin^2(\pi x)\frac{dx}{x}\right] & \text{for } r < R. \end{cases} \tag{12}$$

The radial Schrödinger equation with this potential gives a ground state that is in good numerical agreement with the $m_e/m_h = 0$ curve of Fig. 1. For a finite effective-mass ratio this treatment can legitimately be used for small $\hat{R}$ only, in which case the potential (12) is merely a small perturbation of the Coulomb potential. Using the Coulomb potential as the unperturbed potential and the difference $V(r) + e^2/4\pi\epsilon r$ as the perturbing potential,

first-order perturbation theory yields

$$\hat{E}_b = 1 - \left(\tfrac{4}{9} - \tfrac{2}{3\pi^2}\right)\hat{R}^2 + O(\hat{R}^3). \quad (13)$$

For equal effective masses, it can be checked numerically that this is a reasonable approximation for $\hat{R} < 0.5$. This range of dot radii is so small that the parabolic top is not visible in Fig. 1.

The spatial correlation function

$$C = \frac{\langle(\mathbf{r}_e - \langle\mathbf{r}_e\rangle)(\mathbf{r}_h - \langle\mathbf{r}_h\rangle)\rangle}{\sqrt{\langle(\mathbf{r}_e - \langle\mathbf{r}_e\rangle)^2\rangle\langle(\mathbf{r}_e - \langle\mathbf{r}_e\rangle)^2\rangle}} = \frac{\langle\mathbf{r}_e\mathbf{r}_h\rangle}{\sqrt{\langle r_e^2\rangle\langle r_h^2\rangle}} \quad (14)$$

gives a quantitative measure of correlations. Figure 3 shows the results. For small m_e, as well as for a small dot radius, the particles are weakly correlated, since the electron is essentially in its ground state. And, as could be expected, the correlations are larger in the present case than for an infinite hole offset.

For larger electron mass the correlations increase. The limiting case of a very large mass ratio ($m_e \gg m_h$) can easily be treated in the Born-Oppenheimer approximation, which yields the limiting behavior,[22]

$$C(m_e/m_h \to \infty) \to \frac{\hat{R}}{\sqrt{\hat{R}^2 + 9/(1 - \frac{3}{2}\pi^{-2})}}. \quad (15)$$

The correlation function for the largest mass ratio in Fig. 3 follows (15) extremely well.

B. V_e finite, $V_h = 0$

For finite electron offset, still in a type-I$\frac{1}{2}$ situation, we obtain more accurate results by means of the variational function (9). The results for equal effective masses are given in Fig. 4. For a given offset, the dimension of the quantum dot must have a minimum size in order to be able to bind the electron after the breakup of the exciton. The presence of the hole, however, which in type-I$\frac{1}{2}$ situations merely is a satellite to the electron, makes it possible to have the exciton attached to smaller dots, dots for which the offset potential is insufficient to bind the single electron.[23]

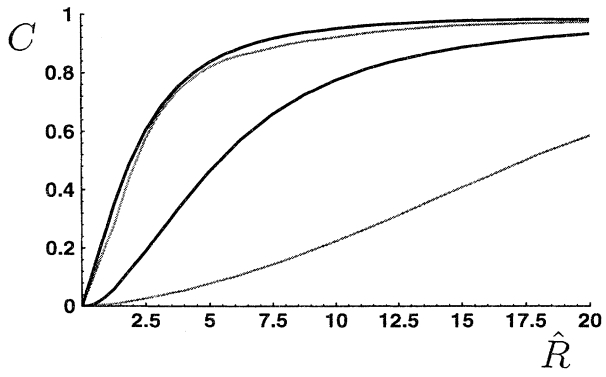

FIG. 3. The spatial correlation function (30) as a function of the dimensionless radius $\hat{R} = R/a_h$ of the quantum dot, for the case $V_e = \infty$. The fully drawn curves correspond to $V_h = 0$, the dashed curves to $V_h = \infty$ (Ref. 16). The two upper graphs correspond to $m_e = 100m_h$, the two lower ones to $m_e = m_h$.

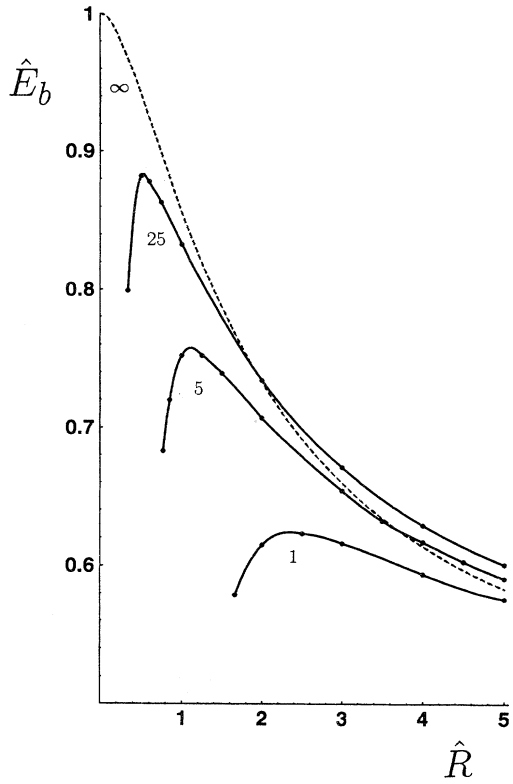

FIG. 4. The dimensionless exciton binding energy $\hat{E}_b$ for $V_h = 0$ and several values of V_e, as a function of the dimensionless quantum dot radius $\hat{R}$. The values of $\hat{V}_e$ are given on the graphs. Here, $m_e = m_h$. In the variational calculation $N_e = 5$ and $N_h = 2$ have been used. The dashed line corresponds to $V_e = \infty$, calculated less accurately with the simpler function (10).

The figure shows that the binding is weaker when the dot is large, and when the offset is low. All graphs show that for a given offset, there exists a radius R_m for which the binding energy is maximal, and R_m increases with decreasing $\hat{V}_e$. This trend can be understood by envisaging the confined particle to create a charge distribution, with which the freely moving particle then interacts. The ground state in a smeared charge distribution deviates from the Coulomb value increasingly more, the more extended the charge distribution is since the overlap decreases. Our interpretation is that the maximum binding energy of the two-particle system corresponds to the minimum extension of the wave function of the confined particle. Since the one-particle ground state in a spherical dot is a well-known textbook example, one can calculate its width $\langle r^2\rangle^{\frac{1}{2}}$ exactly. The width is very large both when the dot is very large, and when the dot is so small that the potential barely binds the electron. Thus,

a *minimum* width of the one-particle ground state must exist for a definite dot radius r_m, and a straightforward calculation[22] yields the exact behavior,

$$\hat{r}_m = c\sqrt{\frac{m_h}{m_e}}\sqrt{\frac{1}{\hat{V}_e}}, \tag{16}$$

with a numerical constant $c = 2.67$. For the offsets $\hat{V}_e = 1, 5$, and 25 in Fig. 4, the binding energy is maximal at dot sizes $\hat{R}_m = 2.35, 1.11$, and 0.53, respectively. This corresponds to the values 2.35, 2.48, and 2.65, respectively, for $\hat{R}_m\sqrt{\hat{V}_e}$, showing that the interpretation of the maxima makes sense, for large offsets even quantitatively.

The binding energy also depends upon the effective masses. As shown in Fig. 5, where $\hat{V}_e = 25$, the binding energy decreases when the electron effective mass becomes smaller. The position of the maximum of $\hat{E}_b$ is seen to increase with decreasing effective mass ratio m_e/m_h in close accordance with the square-root dependence of Eq. (16). Numerically, the maxima in Fig. 5 occur at dimensionless radii 1.63, 1.11, 0.71, and 0.53 for the mass ratios $m_e/m_h = 0.1$, 0.2, 0.5, and 1, respectively, while Eq. (16) yields the values $\hat{r}_m = 1.69$, 1.19, 0.76, and 0.53 for these mass ratios.

Let us consider a specific case. As mentioned above,

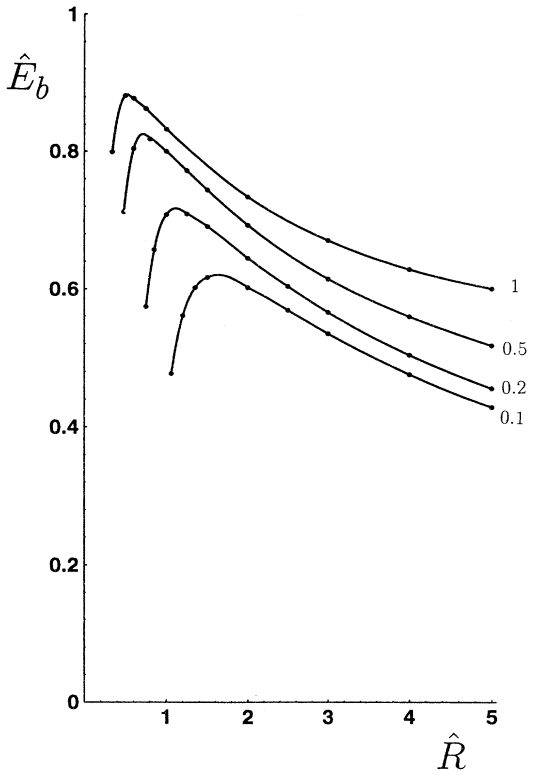

FIG. 5. The dimensionless exciton binding energy $\hat{E}_b$ for $V_h = 0$ and $\hat{V}_e = 25$, as a function of the dimensionless quantum dot radius $\hat{R}$, for several values of the effective-mass ratio m_e/m_h (shown on the right-hand side). In the variational calculation $N_e = 5$ and $N_h = 2$ have been used.

InAs/AlSb is close to a type-I$\frac{1}{2}$ heterostructure. We quote from Ref. 20: "Since the valence band offset of 0.11 eV between InAs and AlSb is so small, we may approximate it as zero, ..." The electron, on the other hand, is well confined in the InAs material, since $V_e = 1.37$ eV.[18] Using[24] an average dielectric constant $\epsilon \simeq 13.6\epsilon_0$, an average light-hole effective mass $m_{h,l} \simeq 0.07m_0$, we find values of the dimensionless electron offset $\hat{V}_e$ to be more than 250, i.e., effectively infinite. Taking the average heavy-hole effective mass to be $m_{h,h} \simeq 0.5m_0$, we find $\hat{V}_e \approx 35$, also very large. The relevant figure is thus Fig. 1. With the electron effective mass in InAs, $m_e = 0.022m_0$, the mass ratios m_e/m_h are about 0.3 and 0.04, respectively. One thus has to interpolate between the mass ratios 0 and 0.5 graphs in Fig. 1. [For the heavy-hole exciton, this can only be used for dimensionless dot radii larger than about 2.3, according to the expression (16). The lower curve in Fig. 5, although corresponding to an offset 25 rather than 35, and a larger mass ratio m_e/m_h, gives also a rough idea of how the binding energy for the heavy-hole exciton depends on the dot radius.]

C. V_e finite, V_h finite

We finally investigate the effect of a finite hole offset. The binding energy as function of the quantum dot radius R is shown in Fig. 6 for several values of the offsets, taken to be equal. Comparison with Fig. 4 shows that the binding energy is smaller when the hole offset is nonzero, as could be expected. We see, moreover, that offsets larger than about 15 yield essentially the same binding energy as infinite offsets.

The figure corresponds to $m_e = m_h$. The binding energy for equal electron and hole offsets is, however, very insensitive to the mass ratio m_e/m_h: Decreasing the mass ratio from 1 to 0.5 lowers $\hat{E}_b$ at most by a few percent. This insensitivity was also found for infinite offsets.[16] However, for a large disparity between the electron and hole offsets, the binding energy is more sensitive to the mass parameters, as witnessed by Fig. 5.

The figure also shows the interesting feature that with increasing values of $\hat{V}_e$, $\hat{E}_b$ now *decreases*, while it *increased* in the absense of the hole offset (Fig. 4). How can this be explained? An increase of any of the two offsets is a positive definite perturbation on the Hamiltonian (1), and leads, therefore, to an increase in its ground-state energy E_0, i.e., gives a negative contribution to the binding energy E_b. Hence, E_b would be lowered if the hole offset were increased for fixed V_e. An increase in the *electron* offset, however, has the additional effect of increasing the electron confinement energy E_c in Eq. (4), and the competition between the two effects determines the change in the binding energy $E_b = E_c - E_0$. The variation of the confinement energy E_c is the dominating contribution when $V_h = 0$ (Fig. 4), but cannot outweigh the combined influence on E_0 from increasing *both* the hole and electron offsets by equal amounts (Fig. 6).

For type-II heterostructures, the offsets are equal if the band gaps in the two materials are equal. For GaAs and InP the band gaps are (at 300 K) 1.42 eV and 1.34

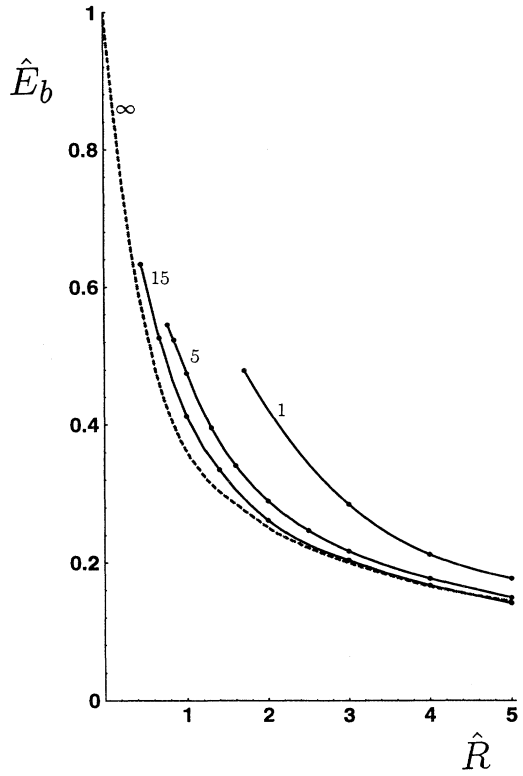

FIG. 6. The dimensionless exciton binding energy $\hat{E}_b$ for equal effective masses and equal offsets, as a function of the dimensionless quantum dot radius $\hat{R}$. The offset values are shown on the graphs. In the variational calculation, $N_e = 3$ and $N_h = 5$ have been used. Results corresponding to $V_e = V_h = \infty$ have been taken from Ref. 16 and are shown as a dashed graph.

eV, respectively.[24] The dielectric constant in both materials is close to $\epsilon = 12.7\epsilon_0$. The band offsets are small, estimated[25] to be of order 0.2 eV and 0.3 eV. Let us assume that this may be approximated by a common offset value of 0.25 eV, and let us assume further that the complications due to strain can be neglected. With an average electron effective mass $m_e \simeq 0.07m_0$, and average light-hole effective mass $m_{h,l} \simeq 0.10m_0$, and the average heavy-hole effective mass $m_{h,h} \simeq 0.54m_0$, we obtain the very rough estimates 30 (light hole) and 5 (heavy hole) for the dimensionless offset values. Thus, the exciton binding energy versus radius graph for offset value 5 in Fig. 6 is relevant for the heavy-hole exciton, and the graph corresponding to the light-hole exciton is squeezed between the two proximate graphs for offset values 15 and infinity. As noted above, the results are insensitive to the value of the mass ratio.

IV. OSCILLATOR STRENGTHS

The hole-electron overlap is a decisive factor in determining the properties of the exciton in optical experiments. Since infinite offsets give zero overlap, the magnitudes of the offsets must clearly be extremely important in type-II situations.

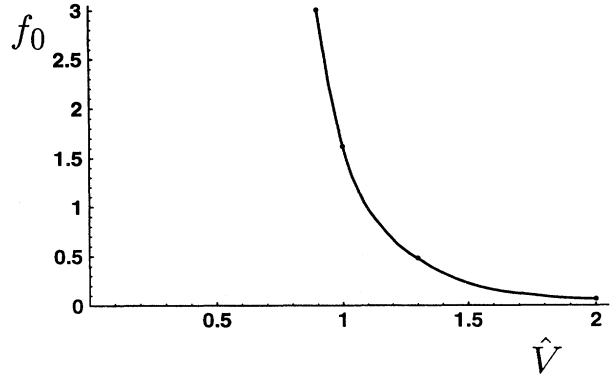

FIG. 7. The overlap factor (17), as a function of the offset. Here, $m_e = m_h$, $\hat{V}_e = \hat{V}_h = \hat{V}$, and $\hat{R} = 3$. In the variational calculation $N_e = 3$ and $N_h = 5$ have been used.

The oscillator strength of an optical transition is proportional to the factor[26]

$$f_0 = \left| \int \psi(\mathbf{r}, \mathbf{r})\, d^3r \right|^2 . \tag{17}$$

Figure 7 shows how the overlap factor f_0 increases dramatically with decreasing offsets. This is expected, of course, since the particles are able to penetrate the dot boundary when the offsets are lowered. In Fig. 8, we illustrate a typical situation, for dimensionless offsets equal to unity, and dimensionless dot radius $\hat{R} = 8$. The marginal electron and hole distributions, obtained from the two-particle wave function, are clearly centered on each side of, and away from, the dot boundary. The tails of these marginal distributions are small *at* the bound-

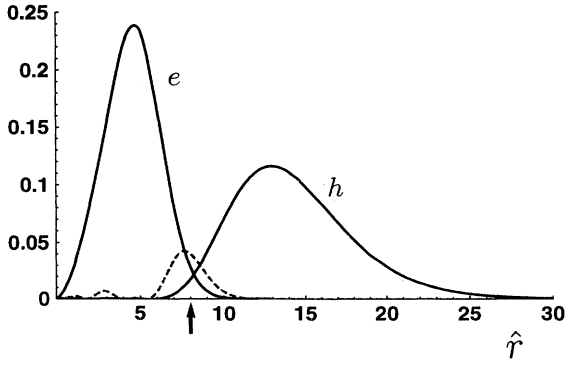

FIG. 8. The radial probability densities $4\pi r_i^2 \psi(r_i)^2$, $i = e, h$ for the electron position (e) and the hole position (h), as functions of the dimensionless distance from the dot center. Here, $\hat{R} = 8$ (indicated by an arrow), $m_e = m_h$, and $\hat{V}_e = \hat{V}_h = 1$. The dashed line shows $10^4 4\pi r^2 \psi(\mathbf{r}, \mathbf{r})^2$. (The small wiggle near $\hat{r} = 3$ is presumably due to numerical inaccuracies.) In the variational calculation $N_e = 3$ and $N_h = 5$ have been used.

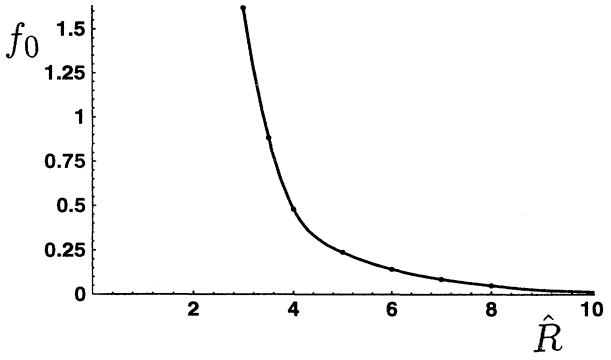

FIG. 9. The overlap factor (17) as a function of the dimensionless dot radius $\hat{R}$. Here, $m_e = m_h$ and $\hat{V}_e = \hat{V}_h = 1$. In the variational calculation, $N_e = 3$ and $N_h = 5$ have been used. The overlap factor will eventually increase, for very large $\hat{R}$, according to (18).

ary, while the overlap, which corresponds to $\mathbf{r}_e = \mathbf{r}_h$, is maximal at, or very close to, the dot boundary.

How the overlap factor depends upon the size of the quantum dot is more interesting. The electron wave function is squeezed out of the dot volume when the radius becomes small enough, just as it is for small offsets. Then the electron and hole are able to correlate, yielding a large overlap function. The decrease of the overlap function with increasing R, shown in Fig. 9, is in accordance with this. However, f_0 must finally increase with R as

$$f_0 \simeq c4\pi\hat{R}^2, \qquad \hat{R} \to \infty, \tag{18}$$

where the constant c depends on the offsets and on the effective-mass ratio. The rationale behind (18) is that for very large radii the exciton will, on the scale of the dot radius, sit very close to the boundary, so that the determination of the wave function is essentially determined through the solution of a plane-wall problem. The plane-wall problem determines the constant c, and the additional factor of $4\pi\hat{R}^2$ in (18) comes from normalization and integration over the dot surface. For the exciton near a plane wall at $z = 0$, we use the simple variational function $\psi(\mathbf{r}_e, \mathbf{r}_h) = (C_e - z_e)(C_h + z_h)e^{-\beta|\mathbf{r}_e - \mathbf{r}_h|}$ for $z_e < C_e$, $z_h > -C_h$, and zero otherwise. For the parameters of Fig. 9, we find for the variational parameters $C_e = C_h = 0.85$ and $\beta = 0.15$, which implies $c = 1.62 \times 10^{-7}$. The rise of f_0 according to (18) is outside the range of radii shown in the figure.

V. SUMMARY

The present work is a model calculation in which we have, in the effective-mass treatment, performed a variational calculation of excitons in spherical quantum dots. We have, in particular, studied how the exciton binding energy E_b depends on the dot radius R, the effective masses m_e and m_h, and the offsets. The nature of the binding energy maximum, as function of the dot radius, is clarified.

ACKNOWLEDGMENTS

We thank G. T. Einevoll for useful remarks. Two of us (U. E. H. Laheld and F. B. Pedersen) are grateful to Norges Forskningsråd for support.

* Electronic address: laheld@phys.unit.no
† Electronic address: borre@phys.unit.no
‡ Electronic address: hemmer@phys.unit.no

[1] G. Bastard, E. E. Mendez, L. L. Chang, and L. Esaki, Phys. Rev. B **26**, 1974 (1982).
[2] R. L. Greene, K. K. Bajaj, and D. E. Phelps, Phys. Rev. B **29**, 1807 (1984).
[3] M. Matsuura and Y. Shinozuka, Phys. Rev. B **38**, 9830 (1988).
[4] T.-F. Jiang, Solid State Commun. **50**, 589 (1984).
[5] R. C. Miller *et al.*, Phys. Rev. B **32**, 8452 (1985).
[6] P. Dawson, K. J. Moore, G. Duggan, H. I. Ralph, and C. T. B. Foxon, Phys. Rev. B **34**, 6007 (1986); K. J. Moore, P. Dawson, and C. T. Foxon, *ibid.* **34**, 6022 (1986).
[7] L. C. Andreani, A. d'Andrea, and R. del Sole, Phys. Lett. A **168**, 451 (1992).
[8] J. W. Brown and H. N. Spector, Phys. Rev. B **35**, 3009 (1987).
[9] Y. Kayanuma, Phys. Rev. B **38**, 9797 (1988).
[10] Y. Kayanuma and H. Momiji, Phys. Rev. B **41**, 10 261 (1990).
[11] For a review, see A. D. Yoffe, Adv. Phys. **42**, 173 (1993).
[12] G. Duggan and H. I. Ralph, Phys. Rev. B **35**, 4152 (1987).
[13] S. V. Branis and K. K. Bajaj, Phys. Rev. B **45**, 6271 (1992).
[14] M. P. Mikhailova and A. N. Titkov, Semicond. Sci. Technol. **9**, 1279 (1994).
[15] J. M. Rorison, Phys. Rev. B **48**, 4643 (1993); Semicond. Sci. Technol. **8**, 1470 (1993).
[16] U. E. H. Laheld, F. B. Pedersen, and P. C. Hemmer, Phys. Rev. B **48**, 4659 (1993).
[17] M. P. C. M. Krijn, Semicond. Sci. Technol. **6**, 27 (1991).
[18] S. Tiwari and D. J. Frank, Appl. Phys. Lett. **60**, 630 (1992).
[19] G. T. Einevoll, Phys. Rev. B **40**, 3410 (1992).
[20] J. D. Dow, J. Shen, and S. Y. Ren, Superlatt. Microstruct. **13**, 405 (1993).
[21] G. T. Einevoll, D. S. Citrin, and Y.-C. Chang, Phys. Rev. B **44**, 8068 (1991).
[22] Details are available upon request to the authors.
[23] U. E. H. Laheld and P. C. Hemmer, Phys. Rev. B **49**, 10 739 (1994).
[24] *Physics of Group IV Elements and III-V Compounds*, edited by K.-H. Hellwege and O. Madelung, Landolt-Börnstein, New Series, Group III, Vol. 17, Pt. a (Springer, Berlin, 1982); *Intrinsic Properties of Group IV Elements and III-V, II-VI and I-VII Compounds*, edited by O. Madelung, Landolt-Börnstein, New Series, Group III, Vol. 22, Pt. a (Springer, Berlin, 1987).
[25] D. D. Nolte, Appl. Phys. Lett. **54**, 259 (1989).
[26] C. H. Henry and K. Nassau, Phys. Rev. B **1**, 1628 (1970).